

Surface analysis on rolling bearings after exposure to defined electric stress

T Zika^{1,3*}, I C Gebeshuber^{1,3}, F Buschbeck¹, G Preisinger², and M Gröschl¹

¹Institute of General Physics, Vienna University of Technology, Vienna, Austria

²SKF Österreich AG, Industrial Electrical Segment, Steyr, Austria

³AC2T Research GmbH, Wiener Neustadt, Austria

The manuscript was received on 5 September 2008 and was accepted after revision for publication on 18 December 2008.

DOI: 10.1243/13506501JET538

Abstract: This article gives an overview about classical and frequency converter-induced spurious bearing currents in induction machines and discusses typical damage patterns caused by the current passage. To investigate on the electric damage mechanisms, test bearings are operated in a test rig and exposed to specific (classical low-frequency, and high-frequency) bearing currents. The induced damages to the surfaces are analysed visually and with the help of an atomic force microscope, and compared for the different electric regimes applied. Further, the electrically damaged bearing surfaces are characterized by standard roughness parameters. The surface structure observable on certain test bearings shows good correlation to the structure found with a bearing that had failed in the field under similar electric conditions. One of the investigated electric regimes applying high-frequency currents proved capable of generating fluting patterns – as found in real applications – on the test rig. The experiments also indicate that high-frequency bearing currents, although in total dissipating less energy, are more dangerous to a bearing than continuous current flow. The presented method gives a good starting point for further investigation on electric current damage in bearings, especially regarding high-frequency bearing currents, and on bearing/grease lifetime under specific electric regimes.

Keywords: bearing currents, variable-speed drives, common-mode voltage, fluting, electric erosion

1 INTRODUCTION

Damages of rolling bearings in electric machines caused by electric current passage are known for decades [1]. The current paths for such parasitic d.c. and low-frequency a.c. bearing currents, which are predominant, e.g. in mains-fed electric machines, have been studied and mitigating methods, such as insulated bearings and shaft grounding brushes [2], have been developed.

Modern induction machines are controlled via fast-switching insulated gate bipolar transistor voltage source converters that, in motors, provide the possibility for precise control and adjustment of

rotational speed and torque as well as energy regeneration at braking operations. In doubly fed induction generators (DFIGs), a frequency converter feeds the rotor windings to enable a constant line frequency at varying rotor speed as well as active and reactive power control [3]. In such electric machines, new types of bearing currents are found. These parasitic high-frequency pulse currents (dV/dt currents, discharge currents, high-frequency circulating currents) affect bearing life to a great extent.

Nowadays, one faces a growing number of wind power applications, where DFIGs are used very frequently. Furthermore, there is an increasing demand for energy-efficient driving applications, commonly utilizing variable-speed drives comprising frequency converters. This leads to an increasing amount of reliability problems of bearings caused by high-frequency electric current passage.

Although both high- and low-frequency currents may reduce bearing lifetime significantly, the sources

*Corresponding author: Institute of General Physics, Wiedner Hauptstraße 8-10/E134, Vienna 1040, Austria.
email: zika@iap.tuwien.ac.at

for these currents are different. For instance, the low-frequency *a.c.* bearing currents are mainly caused by magnetic asymmetries, whereas the high-frequency currents appearing in modern drive systems are mainly caused by the high slew rates of the signals and a non-vanishing common-mode voltage. Hence, the so-called dV/dt currents and other related parasitic effects arise [4].

This article gives an overview about bearing currents in mains-fed as well as frequency converter-controlled induction machines, and their respective sources. Further, the article focuses on the investigation of the damage done to the surfaces of rolling elements and rings of test bearings exposed to various electric regimes. These bearings (thrust ball bearings) were operated in a specially modified test rig, and got exposed to different types of artificial bearing currents (*d.c.*, *a.c.*, and high-frequency pulse currents (HFPCs)). The induced damages are compared on macroscopic and microscopic scales. Besides visual inspection of the macroscopic damage patterns (like fluting or frosting), the running tracks' surface topographies are recorded using an atomic force microscope (AFM). The obtained surfaces are characterized and compared by using standard roughness parameters and, again, visual inspection. This allows for the first time to identify differences in damage induction between classical and modern frequency converter-induced bearing currents. Regarding high-frequency bearing currents, for comparison to damages found in real applications also the surface topography of a bearing operated in wind turbine generator is displayed.

2 TYPES OF BEARING CURRENTS

There are three main causes for bearing currents, namely:

- (a) electrostatic charging;
- (b) magnetic flux asymmetries;
- (c) common mode voltage in combination with high slew rates of the voltage pulses.

The first two phenomena, electrostatic charging and magnetic flux asymmetries, are well known and represent the 'classical reasons' for bearing currents. Non-vanishing common mode voltage in combination with voltage pulses of high slew rates became problematic due to the introduction of modern, fast switching, frequency converters.

In a set-up comprising either an induction generator or motor, electrostatic charging effects may occur because of frictional electricity inside coupled devices. Without insulation of the shafts against each other, a *d.c.* voltage builds up at the motor/generator shaft

(referred to as frame or ground, respectively) and, thus, across the bearings.

Asymmetries in the magnetic field of an induction machine induce an *a.c.* voltage along the shaft in the axial direction. When the bearings are in conductive or resistive state of impedance [5], this voltage drives a so-called *circulating current* along the shaft, across one bearing, through the frame of the machine, and across the other bearing back to the shaft. The path may eventually extend across the bearing of a driven machine, depending on local impedance conditions. These currents are of low-frequency nature, according to the fundamental frequency of the phase voltages. They generate dissipative (active) power inside a bearing, which is locally converted into heat. Thereby, the surfaces as well as the lubricant of the bearing could be damaged.

In modern frequency converter-controlled systems, the phase signals are composed of voltage pulses of high slew rates (typically 2–10 kV/ μ s). Similar voltage transitions are characteristic for the common mode voltage and the voltage at the motor star point. If a capacitance is present in the considered circuit, current pulses $I = C dV_1/dt$ are generated each time during the transitions of the phase voltage V_1 . (The same applies for phase voltages V_2 and V_3 .) These currents are of high-frequency nature and are often referred to in the literature as ' dV/dt currents'. Further, according to Mütze [6] and Ollila *et al.* [7], these dV/dt currents are capable of driving high-frequency circulating currents with a current path including the shaft, both bearings, and the motor frame.

Figure 1 shows a sketch of an induction motor with the associated stray capacitances (Fig. 1(a)) and the respective electric equivalent circuit diagram, with respect to frequency converter-induced currents (Fig. 1(b)). In such a set-up comprising an induction motor, the frequency converter applies pulse width modulated (PWM) voltage patterns to the stator windings. Hence, the voltages at the stator windings and the (unavoidable) stray capacitances between the stator windings and the rotor (shaft) are mainly responsible for the formation of parasitic currents.

During transitions of the phase voltage V_1 , the current $I_{SF} = C_{SF} dV_1/dt$ flows via the stray capacitance C_{SF} from the stator windings to the motor frame (Fig. 1(b)). Accordingly, the current I_{SR} flows from the rotor winding through C_{SR} to the rotor (shaft) and then splits into a branch through C_{RF} (I_{RF}) and branches through the motor bearings (I_{B1} , I_{B2}), depending on the bearings' actual state of impedance. Therefore, a high-frequency pulse-shaped voltage $V_{RF} = V_{B1,2}$ is created between the rotor (shaft) and the machine's frame and, thus, across the bearings. If both bearings operate in the full-film lubrication regime (capacitive state of impedance), $V_{B1,2}$ can be estimated (with neglect of V_{PE1} see

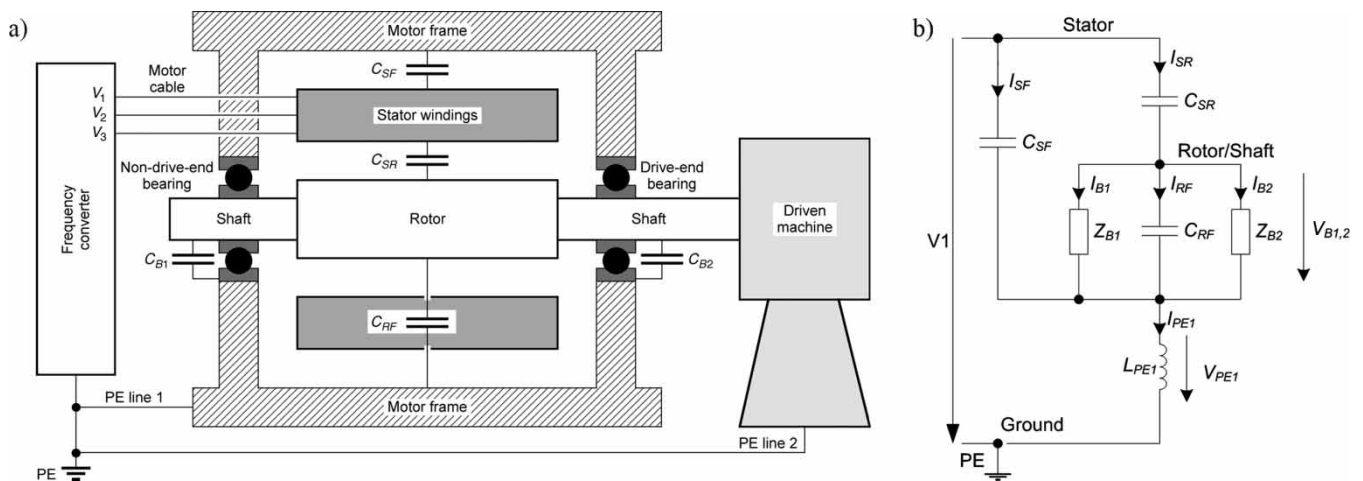


Fig. 1 (a) Sketch of an induction motor with associated stray capacitances and (b) electric equivalent circuit of an induction motor. Only the relevant electric parts responsible for HFPCs are shown

below) by considering the purely capacitive voltage divider as

$$\frac{V_{B1,2}}{V_1} \approx \frac{C_{SR}}{C_{SR} + C_{RF} + C_{B1} + C_{B2}}$$

with the bearing capacitances C_{B1} , C_{B2} replacing the more general impedances Z_{B1} and Z_{B2} in Fig. 1(b). From the motor frame, the summing current $I_{PE1} = I_{SF} + I_{SR} = I_{SF} + I_{RF} + I_{B1} + I_{B2}$ flows back to the converter via the PE line. Thereby, it creates a voltage V_{PE1} across the inherent inductance L_{PE1} of the line, according to $V_{PE1} = L_{PE1} dI_{PE1}/dt$. These voltage peaks V_{PE1} are coupled to the rotor (shaft) via C_{RF} . Basically, this has no effect on the bearing voltage $V_{B1,2}$, because it results in a common potential shift of the motor frame and shaft.

If a coupled device (like a gearbox or a driven machine) is present without an electrical insulation against the motor shaft, another branch exists for a dV/dt current through the bearings of the coupled device. Depending on the grounding situation of the coupled device, this may cause or pronounce parasitic currents, and also harm the bearings of the coupled device.

As long as a bearing operates in the full-film lubrication regime and, thus, from the electrical point of view acts as a pure capacitance, any current flowing through the bearing is purely reactive and does not cause any physical effect such as heating, etc. However, if the bearing operates in a resistive state of impedance [5], any current flow is connected to the generation of active power. Hence, the bearing could suffer damage to the lubricant and to its surfaces. Such active current flow occurs if the bearing is not in the full-film lubrication regime at the time of the converter's switching operations, or if the insulating lubricant film breaks down while the stray capacitances inside the electric machine are charged (this charging of the stray

capacitances is basically also caused by the dV/dt currents).

3 DAMAGE PATTERNS

Parasitic currents flowing through a bearing may be harmful in various ways. Classical low-frequency bearing currents induce damage on the surfaces of the raceways and rolling elements. This mainly results in a darkening of the running tracks (Fig. 2(b)), which in the end may lead to a macroscopic washboard-like pattern, also called fluting (Fig. 2(d)). Kohaut [1] tries to explain this phenomenon by the bearing balls being forced to 'jump' over electric pittings that were not flattened ideally. This leads to oscillations of the rolling elements and finally causes the raceway surface to develop a washboard pattern. Despite this qualitative explanation, Mütze *et al.* [8] states that it is still unclear why certain bearings operated under identical conditions show fluting and others do not. Furthermore, also the grease of the bearing gets burned by the current flow and shows a blackened appearance (Fig. 2(a)).

In electric drive systems comprising a frequency converter, the current flow through the bearings is not continuous, but occurs in discrete pulses. These pulses are either synchronized with the switching operations of the frequency converter (dV/dt currents) or distributed stochastically whenever the electrically insulating lubricant film between rings and rolling elements breaks down (discharge currents [9, 10]). These HFPCs result in a different visual appearance of the damaged running tracks compared to the continuous classical bearing currents. The running tracks macroscopically show a grey/dull appearance, also known as 'frosting' (Fig. 2(c)), caused by microscopic craters all over the raceway surface. However, in the end this kind of surface damage may also lead to a

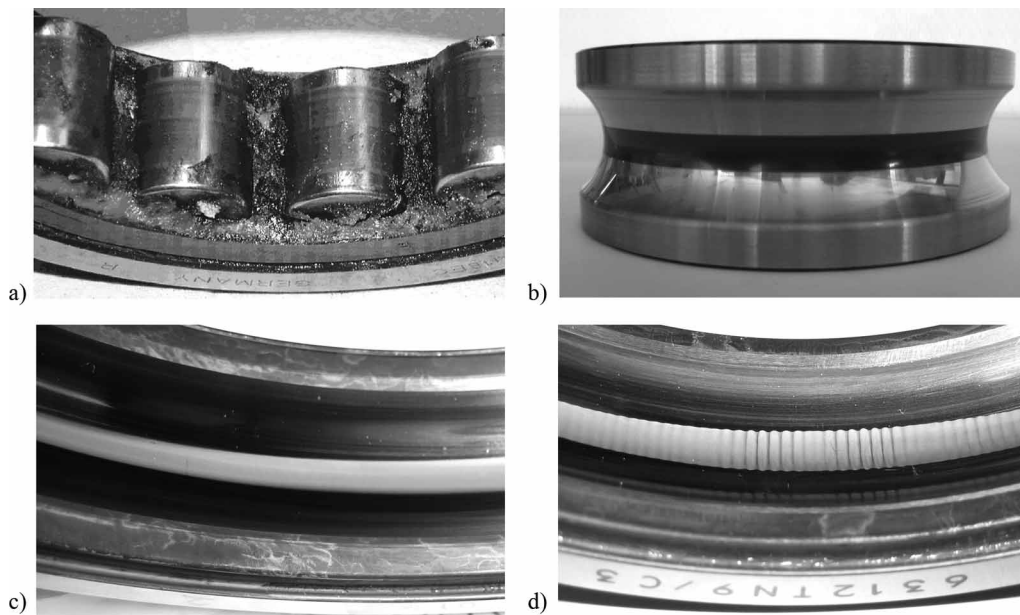


Fig. 2 Bearing damages: (a) blackened grease; (b) darkened running track; (c) grey/dull (frosting) running track; and (d) fluting pattern

washboard/fluting pattern (Fig. 2(d)) on the affected surfaces.

4 EXPERIMENTAL SET-UP

To investigate the different effects of various electric regimes onto the bearings' surfaces, a number of test specimens have been created in several test runs. As specimens thrust ball bearings were used, mainly because of easier and more flexible experimental handling (disassembling and reassembling). These bearings (type 51305) are made of 100Cr6 bearing-grade steel. All sample bearings were lubricated with the same amount of standard grease consisting of mineral base oil and lithium soap-based thickener. Furthermore, exactly the same experimental procedure in all test runs was ensured by fully automated test run control.

4.1 Mechanical set-up

A thrust ball bearing test rig available at SKF Österreich AG, Steyr, Austria, was modified to allow the application of specific electric regimes on the test bearings (see Fig. 3). The support bearings were hybrid ones; the shaft (and hence the shaft washer of the test bearing) was contacted by a rotating mercury contact. The loaded housing washer was insulated against the test rig using a polyamide disc and contacted by a brass screw going through this insulating layer. The mechanical load was applied via a lever/spring combination and measured with a load cell. The running temperature of the bearing could not be controlled but was

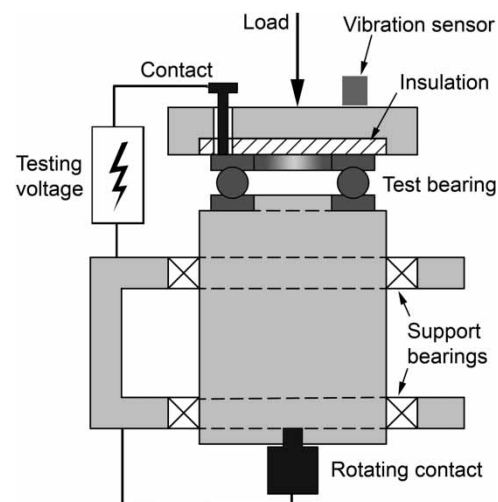


Fig. 3 Sketch of the test rig's mechanical set-up

measured at the housing washer using a thermocouple. Finally, bearing vibrations were also monitored utilizing a piezoelectric acceleration sensor (sensor Brüel & Kjaer-type 4367, conditional amplifier Brüel & Kjaer-type 2626). To allow comparison between experiments, the RMS values of the measured acceleration signal were normalized to the values found at the very beginning of the respective experiment. These normalized values are marked as 'vibration level' in Fig. 4.

4.2 Experimental procedure

From the mechanical point of view, all test bearings were operated at 1000 r/min rotational speed

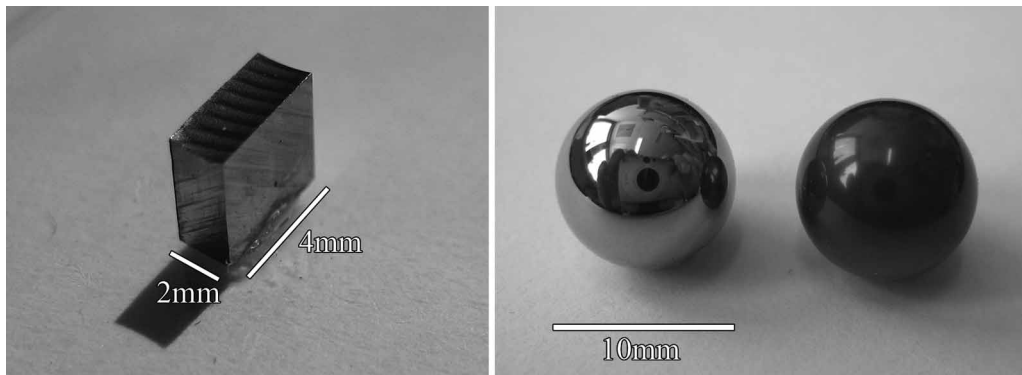


Fig. 4 Samples for AFM analysis; left picture: sample cut out of a washer's running track (approx. $2 \times 4 \text{ mm}^2$, HFPC_2); right picture: two rolling elements (left: virgin condition, right: 3 A *a.c.*)

and at a load of 1400 N. First, there was a running-in phase lasting for 2 h, where no electric stress was applied to the bearing. Afterwards, the desired electric regime was engaged and the bearing was operated for 24 h under the respective electric regime. After 26 h of total running time each test run was stopped automatically.

4.3 Electric regimes

The effects of five different electric regimes have been investigated: for reference one without any current, two regimes applying continuous (classical) currents, and two regimes applying discrete current pulses (simulating frequency converter-induced currents). For the two continuous (classical) current regimes, a current of 3 A (RMS) was chosen to induce damage in the bearings. Considering the Hertzian contact area of the test bearings, this resulted in a current density of 1.8 A/mm^2 , which is above the limits for induction of damage commonly stated in the literature [5]. An overview including the associated energy (per single pulse and over the whole test run) and power (effective and peak) values is shown in Table 1.

The following designations will be used hereafter to specify the electric regime applied to the test bearing.

Table 1 Electric energy and power values for the various regimes applied to the test bearings

Electric regime	Single pulse energy (J)	Total accumulated energy (kJ)	Effective power (W)	Peak power (W)
WO	–	0	–	–
DC	–	233	2.7	2.7
AC	–	181	2.1	3.5
HFPC_1	9×10^{-7}	0.778	0.009	8
HFPC_2	6.8×10^{-5}	58	0.68	50

1. WO: no active electric regime is applied to the bearing, so there is no current flow through the bearing.
2. DC: a 3-A continuous *d.c.* current source is connected to the bearing. The anode is at the housing washer. The voltage drop across the bearing is about 0.9 V. This amounts to a power of 2.7 W and a total accumulated energy of 233 kJ.
3. AC: a 3-A (RMS) continuous *a.c.* current with a frequency of 50 Hz is applied to the bearing. Measurements show a power of approximately 2.1 W and a total accumulated energy of 181 kJ.

To apply HFPC, specially designed electronics are attached to the bearing. These electronics simulate the current pulses delivered by a frequency converter using a capacitor for coupling such pulses to the test bearing. The electric energy is applied to the bearing in a short period of time with comparably long idle periods in between the single pulses. This leads to big peak power values (at the times of the pulses) and lower values for the effective power over time (see Table 1). In this article, two different versions of such HFPCs are reported.

1. HFPC_1: the coupling capacitor is in the order of some nF. This results in a peak pulse current of approximately 1.5 A. The repetition frequency is 10 kHz. The accumulated total energy amounts to 778 J.
2. HFPC_2: The coupling capacitor is in the order of a few μF . This results in a peak pulse current of approximately 20 A. The repetition frequency is 10 kHz. The accumulated total energy amounts to 58 kJ.

It has to be noted that the electric impedance of a bearing may fluctuate in the course of such a test run. Therefore, the data given in Table 1 are extrapolated over the total test run duration using starting values measured at the beginning of the respective test run.

5 ANALYSIS PROCEDURE

To obtain a first impression of the electrically induced damages to the test specimens, photographs of the test bearings were taken to assess the macroscopic damage patterns. Then, AFM pictures of the respective surface topographies were recorded and flattened using a second-order polynomial fit to remove the curvature of the sample. For each sample, the running tracks on the shaft and housing washer as well as on one of the rolling elements have been examined. To do so, the washers had to be cut into smaller samples using a cut-off wheel, whereas the surfaces of the rolling elements could be investigated without further manipulation (Fig. 4).

Using the topography data obtained with the AFM, the surfaces were also judged visually. Standard roughness parameters were used to characterize the surface: R_q (RMS roughness) and R_t (spread between the highest and lowest height values) roughness values were calculated using the full $30 \times 30 \mu\text{m}^2$ AFM scan of the surface, where $R_q = \sqrt{\frac{1}{n} \sum_{i=1}^n y_i^2}$ and $R_t = \max y_i - \min y_i$ (y_i represent the height values of the scanned surface).

For reference, topography analysis was also performed on a virgin bearing.

6 RESULTS

The data collected during the test runs show that all test bearings had endured a mechanical load of approximately 1450 N throughout their respective test run. A slight increase of the initially set load of 1400 N was most likely caused by the increase in bearing and test rig temperatures. Bearing temperature data reveal that all bearings did run in a temperature range from 45 to 55 °C.

Analysis of the online vibration measurement data of the test runs (Fig. 5) shows that the specimen HFPC_2 exhibited a huge increase in vibration level, beginning after 8 h of running time. In contrast, all

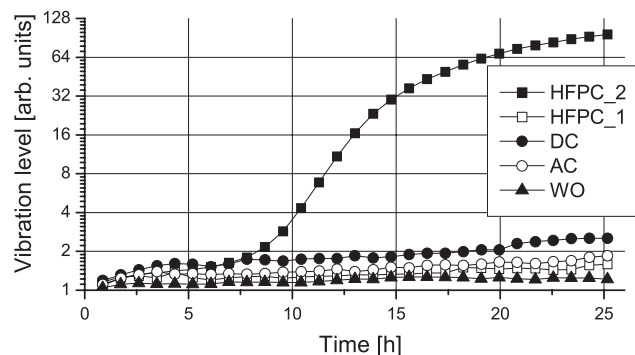


Fig. 5 Progression of the vibration level of the sample bearings

other specimens (WO, AC, DC, and HFPC_1) showed less pronounced levels of vibration.

Figure 6 shows photos of the specimens HFPC_2, HFPC_1, and AC. For all test bearings, the shaft washers have much broader running tracks than the housing washers. With bearing HFPC_2 one can clearly see a fluting pattern that developed on the shaft washer only. This fluting pattern consists of bright flutes separated by darker areas in between them (this pattern is also observable in Fig. 4, left). The corresponding housing washer and the rolling elements only show a strong discolouring. Bearing HFPC_1 shows a dull running track (frosting) on both washers. The rolling elements, however, do not show significant 'frosting'. Bearing AC shows a very dark discolouring on both washers and on the rolling elements. The DC bearing (not shown) looks very similar to the AC bearing, whereas the WO bearing only shows very slight tracks in the raceways (see Fig. 7). The virgin bearing REF naturally shows no signs of wear in the raceways or on the rolling elements.

In Fig. 7, the surfaces of a virgin bearing's shaft washer and the shaft washer of the test bearing WO, run without any current passage, are shown. In both cases one can clearly see the initial honing pattern, which has its origin in the production process. The WO bearing's surface shows some marks. It also has less surface roughness (R_q and R_t , see Tables 2 and 3). This is also valid for the housing washers of these bearings, whose topographies have a similar appearance to those of the shaft washers. The rolling elements do initially have very smooth surfaces. However, even here the surface roughness (R_q and R_t) is reduced further due to bearing operation without electric stress.

Figure 8 depicts the surface of the HFPC_2 bearing's shaft washer. In the left picture the bright zone of the fluting pattern is shown. The honing pattern, as seen on the bearings REF and WO, has completely vanished. The surface shows discrete sphere-shaped features up to approximately $2 \mu\text{m}$ in diameter. The right picture shows the dark zone of the fluting pattern. Here, discrete features are less distinct. Furthermore, the roughness is much less compared to the brighter zone (see also Tables 2 and 3). The housing washer and the rolling elements of this bearing show similar structures as the shaft washer.

The surface of the HFPC_1 bearing's shaft washer is shown in Fig. 9 (left picture). It reveals similar features as the HFPC_2 bearing, but on a smaller scale. The discrete sphere-shaped features have an approximate diameter of $1 \mu\text{m}$. From the optical impression, this bearing's rolling element (see Fig. 6) shows only little change to its original surface. Nonetheless, the surface topography (Fig. 9, right) already reveals damaged areas, which are not covering the whole surface, yet. In the other regions the rolling element still exhibits similar structures as for the WO bearing.

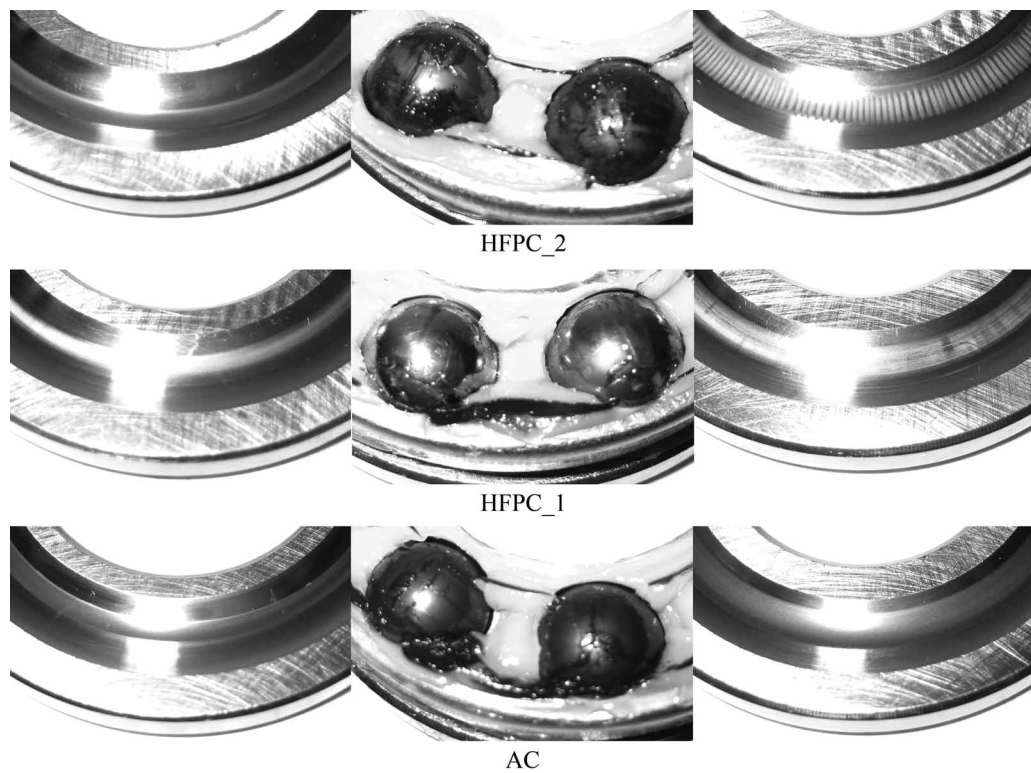


Fig. 6 Photos of the test bearings (HFPC_2, HFPC_1, and AC) demonstrating the induced damage (left to right: housing washer, rolling elements+grease, shaft washer)

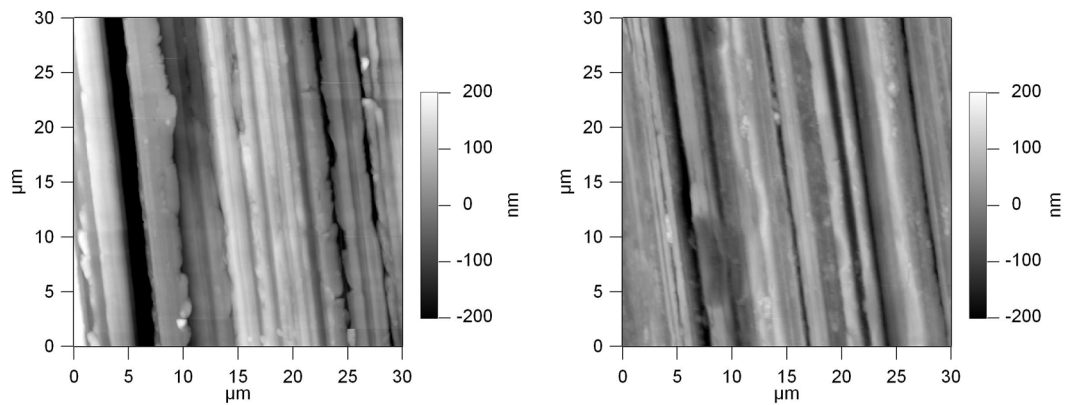


Fig. 7 Comparison of the shaft washers' surface topography of bearings REF (left picture) and WO (right picture)

Table 2 R_q roughness of washers and rolling elements of test bearings

R_q (nm)	Housing washer	Shaft washer	Rolling element
REF	112	112	10
WO	61	64	7
DC	56	91	81
AC	60	78	83
HFPC_1	62	63	24
HFPC_2 (bright spot)	90	128	58
HFPC_2 (dark spot)	–	45	–

Table 3 R_t roughness of washers and rolling elements of test bearings

R_t (nm)	Housing washer	Shaft washer	Rolling element
REF	843	754	116
WO	419	399	98
DC	685	921	833
AC	624	792	944
HFPC_1	475	450	293
HFPC_2 (bright spot)	606	838	585
HFPC_2 (dark spot)	–	480	–

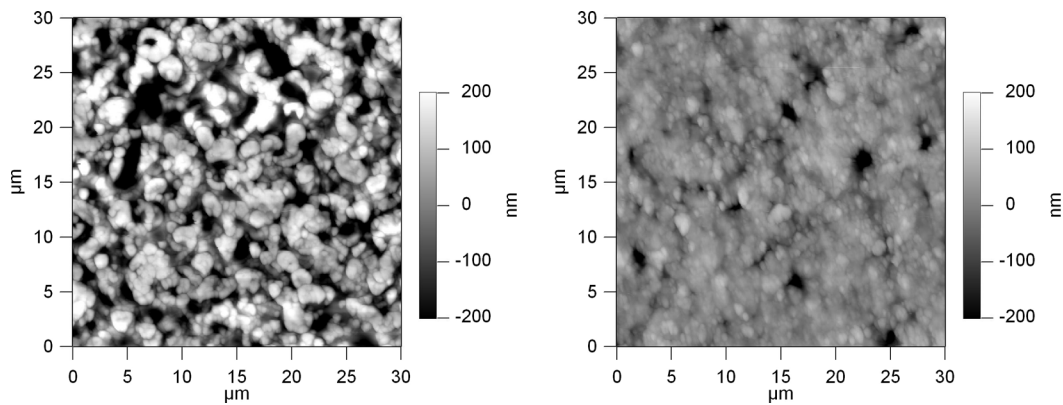


Fig. 8 Comparison of surface topography of HFPC_2 test bearing; left picture: bright spot in fluting pattern; right picture: dark spot in fluting pattern

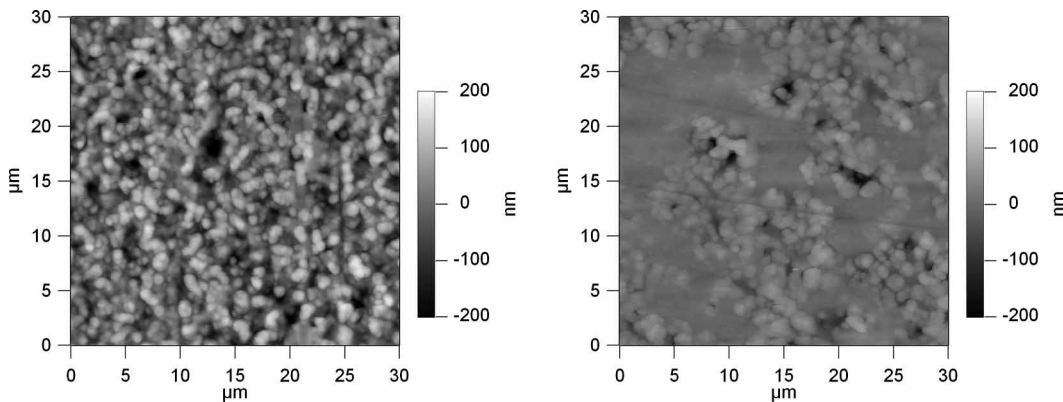


Fig. 9 Topography of HFPC_1 test bearing; left picture: surface of the shaft washer; right picture: surface of a rolling element

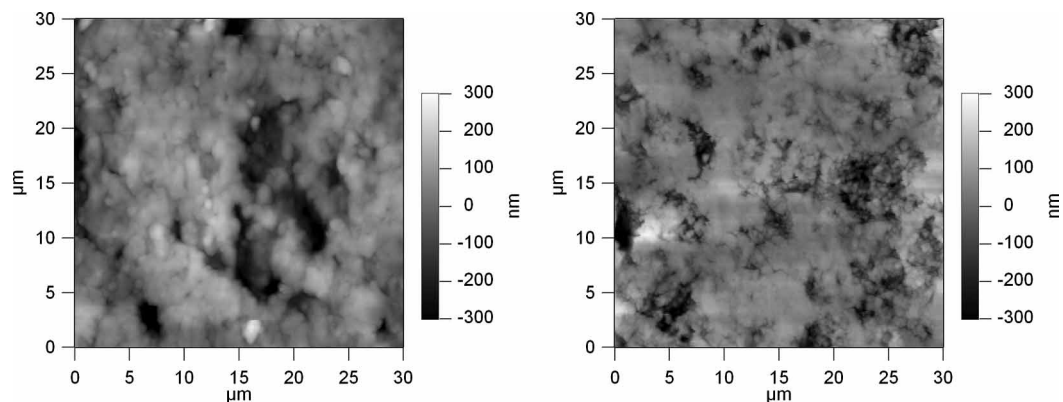


Fig. 10 Comparison of the shaft washers' surface topography of bearings DC (left picture) and AC (right picture)

In Fig. 10, the shaft washer surfaces of the test bearings DC and AC are compared. Both bearings' surfaces do not show honing patterns anymore. In contrast to the HFPC test bearings, these two specimens do not show such well-defined features, but exhibit a cloudy surface structure.

As a reference to the field, Fig. 11 shows the surface topography of a deep-groove ball bearing that was

operated in a wind turbine generator. The surface of this bearing's outer ring shows clear similarities to the HFPC test bearings' surfaces. The discrete features in this case have a diameter of 3–5 μm .

The R_q roughness values of the various samples are listed in Table 2. The WO bearing shows reduced R_q values compared to the virgin bearing's (REF) values. Especially the washers' values are nearly halved.

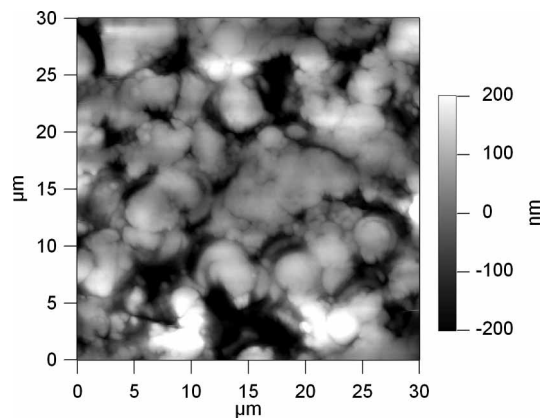


Fig. 11 Surface topography of a large-size deep-groove ball bearing's outer ring that was operated in the field (wind turbine generator)

The DC and AC bearings show very similar R_q values for housing washer and rolling elements. The R_q values of the rolling elements are higher than the REF bearing's value.

The R_q roughness of bearing HFPC_1 is still very similar to the one of bearing WO, even though the structure on the surface is significantly different (compare Figs 7 and 9). Only the rolling elements show a significant difference in the R_q value.

Inside the bright spots of bearing HFPC_2, the R_q values on the washers are significantly increased with respect to the other test bearings and are comparable to the values of the REF bearing. The roughness values of the rolling element do not reach the ones of the AC and DC bearings, but are high compared to all other test bearings. The dark spot in the fluting pattern, on the contrary, shows low R_q values, even lower than that for the WO bearing's shaft washer.

The same applies to the R_t roughness values seen in Table 3, with the exception that the values for HFPC_2 are lower than the ones for AC and DC.

7 DISCUSSION

Various test runs were conducted in which bearings were damaged by different electric regimes. In the course of such a test run, the AC and DC electric regimes applied more electric energy to the bearing than the HFPC_2 regime. Having this in mind, it is astonishing that the HFPC_2 test bearing is the only bearing showing a fluting pattern in one of the raceways. The generation of this fluting pattern can be clearly observed from the vibration measurement data (Fig. 5), where after 8 h of running time a significant rise in vibration level sets in. All other test bearings are inconspicuous in terms of vibration level and show similar values. These findings of on-line vibration monitoring are confirmed by the macroscopic impression of the test bearings after the test runs. All

other test bearings do not show a fluting pattern in any raceway.

In general, the HFPC regimes (HFPC_1 and HFPC_2) apply the electric energy in a very short period of time (during the current pulse, 50 ns up to some μ s) with long idle times without any current flow in between the single pulses. This results in comparatively low effective power and energy values, in contrast to high peak power values. These peak power values are higher than the ones of the continuous current (AC or DC) regimes (see values in Table 1). The fact that the HFPC_2 test bearing suffered the most severe damage (fluting) indicates that not only the overall applied energy but also the peak power is of importance regarding the damaging process. The HFPC regimes deposit the electric energy in a short period of time. Therefore, the affected surface area in a single pulse is small and well localized. However, after a certain time of running many of these single localized areas accumulate and the damage is spreading across the whole surface. With the continuous current regimes, on the other hand, the energy is more evenly distributed across the surfaces of the bearing's running tracks and rolling elements immediately. However, further research is necessary to entirely clarify why the pulsed application of electric energy is capable of inducing a fluting pattern in shorter time than higher-energetic *a.c.* or *d.c.* currents.

The AFM topography pictures of the test bearings clearly bring out the difference in damage mechanism between continuous current flow and pulsed current flow. The surfaces of the AC and DC bearings share a cloudy structure without discrete features. Both HFPC test bearings, on the contrary, show distinct sphere-shaped features on their surfaces, presumably induced by the discrete current (energy) pulses. For reference, also a deep-groove ball bearing that had been operated in a wind turbine generator was examined. In this type of application, bearings are exposed to HFPCs. Although the geometric dimensions and other mechanical parameters between this bearing and the other sample bearings investigated here are not directly comparable, the surface structures observed on both HFPC test bearings show good correlation to the features found on the bearing from the field. The bearing run without any current still exhibits the honing structure originating in the production process. However, the test run did, as one would expect, burnish the surface roughness compared to the topography of a virgin bearing. All test bearings that were exposed to any electric regime do not show signs of this honing pattern anymore, which is a hint that complete remelting of the surfaces has occurred. The HFPC_1 bearing's rolling element shows only certain areas that had been exposed to the pulsed currents and other areas exhibiting the initial surface. Using longer running times, one could expect that the whole surface will be covered with electrically induced

damage pattern. It is also interesting that the areas showing damage consist of cavities below the surrounding undamaged surface, but also hills reaching above the initial surface.

Unfortunately, the typical roughness parameters R_q and R_t only represent an insufficient description of the bearings' surfaces regarding current damage, because these parameters are neglecting the actual surface structure to a great extent. The WO bearing's surfaces are burnished by the mechanical running. This can be observed by a reduction of the WO bearing's roughness parameters compared to the REF bearing. Both roughness parameters do show increased values for the AC, DC, and HFPC_2 bearings when compared to the WO bearing. However, the virgin bearing (REF), due to the distinctive honing structure shows values of similar level to the AC, DC, and HFPC_2 test bearings. Furthermore, the values of the HFPC_1 bearing's washers do not significantly differ from the WO bearing's ones, only the roughness values for the rolling elements are elevated. This is neglecting the fact that the complete surface structure of the HFPC_1 bearing has been transformed by the electric stress.

The HFPC_2 fluting pattern is macroscopically made up of bright (topographically lower) and dark (topographically higher) regions. It is remarkable that the respective surfaces also have a considerably different microscopic appearance, regarding surface topography and roughness. Although the bright areas do show a structure with discrete features (as discussed above) and also high R_q and R_t roughness values, the dark areas do not show many distinct features and the roughness parameters are very low. Here, also other microscopic parameters, e.g. micro-hardness and chemical composition, might be of interest in order to further understand the mechanism behind the generation of this fluting pattern.

8 CONCLUSION

An overview was given about the different types of bearing currents in induction machines. Typical macroscopic damage patterns caused by electric current passage have been discussed. Test bearings were exposed to various electric regimes (*a.c.*, *d.c.*, and HFPCs) and the resulting damages were assessed by visual inspection and by using an AFM. The differences of classical continuous bearing currents (*d.c.* or *a.c.*) to the more recent frequency converter-induced HFPCs have been exemplified with the help of AFM surface topography measurements on the test bearings. Furthermore, it could be illustrated that both HFPC test bearings show similar features like a reference bearing that had been exposed to frequency-converter-induced currents in the field. Damaged bearing surfaces have been characterized by typical surface roughness parameters R_q and R_t . However,

these parameters turned out not to be fully suitable to characterize damage by electric current passage, since the surface structure is neglected to a great extent. Therefore, other ways of surface characterization have to be found.

The experiments also showed that HFPCs are capable of generating fluting damage to the surface in shorter times compared to continuous currents of higher energy. However, especially regarding the fluting damage, closer investigations are still necessary to clarify the exact mechanism of its induction. Here, the surface topography pictures give a first hint for a different surface structure in the bright and in the dark areas of the pattern.

To sum up, the presented experiments are a good starting point for further investigation on electric current damage in bearings, regarding the damaging mechanism of HFPCs, thresholds for damage induction, generation of fluting patterns, and bearing/grease lifetime under specific electric regimes.

ACKNOWLEDGEMENTS

This work was funded from the Austrian Kplus-Program and has been carried out within the Austrian Center of Competence for Tribology, Wiener Neustadt, Austria. The authors wish to thank H. Köttritsch and H. Weninger from SKF Österreich AG, Development Centre Steyr, Austria, and H. Stache, R. Spallek and S. Grundei from Klüber Lubrication München KG, Munich, Germany, for valuable discussions and their support of this work.

REFERENCES

- 1 Kohaut, A. Riffelbildung in Wälzlagern infolge elektrischer korrosion. *Z. Angew. Phys.*, 1948, **1**(5), 197–211.
- 2 Hausberg, V. and Seinsch, H. O. Schutzmaßnahmen gegen Lagerschäden umrichter gespeister Motoren. *Electr. Eng.*, 2000, **82**, 339–345.
- 3 Ehlert, D. and Wrede, H. Wind turbines with doubly fed induction generator systems with improved performance due to grid requirements. In Proceedings of the Power Engineering Society General Meeting, 24–28 June 2007.
- 4 Busse, D., Erdman, J., Kerkman, R., Schlegel, D., and Skibinski, G. Bearing currents and their relationship to PWM drives. *IEEE Trans. Power Electron.*, 1997, **12**(2), 243–252.
- 5 Preisinger, G. *Cause and effect of bearing currents in frequency converter driven electrical motors – investigations of electrical properties of rolling bearings*. Dissertation, TU Wien, 2002.
- 6 Mütze, A. *Bearing currents in inverter-fed AC-motors*. Dissertation, TU Darmstadt, Shaker Verlag, Aachen, 2004.
- 7 Ollila, J., Hammar, T., Iisakkala, J., and Tuusa, H. On the bearing currents in medium power variable speed AC

drives. In Proceedings of the IEEE International Conference on Electric Machines and Drives, Milwaukee, WI, USA, 18–21 May 1997, pp. MD1/1.1–MD1/1.3.

- 8 Muetze, A., Binder, A., Vogel, H., and Hering, J.** What can bearings bear? *IEEE Ind. Appl. Mag.*, 2006, **12**(6), 57–64.
- 9 Kempfski, A.** Capacitively coupled discharging currents in bearings of induction motor fed from PWM (pulse width modulation) inverters. *J. Electrostat.*, 2001, **51–52**, 416–423.
- 10 Chen, S. and Lipo, T. A.** Source of induction motor bearing currents caused by PWM inverters. *IEEE Trans. Energy Convers.*, 1996, **11**(1), 25–32.

APPENDIX

Notation

C_{B1}, C_{B2}	capacitance of a bearing	C_{SR}	capacitance between the stator and the rotor
C_{RF}	capacitance between the rotor and the frame	I_{B1}, I_{B1}	current flowing through the bearing
C_{SF}	capacitance between the stator and the frame	I_{PE1}	current flowing in the protective earth line
		I_{RF}	current flowing from the rotor to the frame
		I_{SF}	current flowing from the stator to the frame
		I_{SR}	current flowing from the stator to the rotor
		L_{PE1}	inductance of the protective earth line
		R_q	RMS roughness
		R_t	spread between the highest and the lowest surface height values
		V_{B1}, V_{B2}	voltage across a bearing
		V_{PE1}	voltage drop in the protective earth line
		V_{RF}	voltage between the rotor and the frame
		V_1, V_2, V_3	phase voltages of the induction machine
		y_i	height values of the surface topography
		Z_{B1}, Z_{B1}	impedance of a bearing